Science Advances
AAAS

advances.sciencemag.org/cgi/content/full/6/28/eabb2891/DC1

Supplementary Materials for

Smart, soft contact lens for wireless immunosensing of cortisol

Minjae Ku, Joohee Kim, Jong-Eun Won, Wonkyu Kang, Young-Geun Park, Jihun Park, Jae-Hyun Lee, Jinwoo Cheon*, Hyun Ho Lee*, Jang-Ung Park*

*Corresponding author. Email: jang-ung@yonsei.ac.kr (J.-U.P.); hyunho@mju.ac.kr (H.H.L.); jcheon@yonsei.ac.kr (J.C.)

Published 8 July 2020, *Sci. Adv.* **6**, eabb2891 (2020)
DOI: 10.1126/sciadv.abb2891

The PDF file includes:

Other Supplementary Material for this manuscript includes the following:

(available at advances.sciencemag.org/cgi/content/full/6/28/eabb2891/DC1)

Supplementary Materials and Methods

Fabrication of the graphene sensor of FET structure

The Cr/Au electrode was thermally evaporated as 5/100 nm thickness and patterned to form the source and drain electrodes photolithographically. The distance between them is the length of the channel, i.e., 560 μm. After the source and drain were formed, graphene was water-transferred onto the source and drain. Chemical vapor deposited (CVD) graphene was purchased from Graphene square. The large-area graphene that was deposited on the Cu foil was cut to the desired size and spin-coated with the poly (methyl methacrylate) (MicroChem Corp., 950 PMMA C2). The PMMA that was coated on the underside of the graphene unintentionally was rinsed with acetone. Then, the graphene was floated on the Cu etchant ($FeCl_3$:HCl:H_2 = 1:1:20 vol%) to etch the Cu foil on the underside of the graphene. When the etching was finished, the etchant remained and the PMMA was removed by rinsing with DI water. After the rinsing, the graphene was transferred to the desired site, i.e., between the source and drain, and patterned to the sizes of 120 μm width and 560 μm length by photolithography and reactive ion etching (RIE) (50 W, 40 sccm, 120 s).

Fabrication of the AgNF-AgNW hybrid antenna

An AgNF-AgNW electrode was formed by electrospinning and subsequent electrospraying. The AgNFs were formed by electrospinning for 10 seconds using a suspension of Ag nanoparticles (NPK, Korea, average diameter: 40 ± 5 nm, solvent: ethylene glycol, concentration: 50 wt.%) on the substrate, at the following conditions. The inner and outer diameters of the nozzle were 0.34 and 0.64 mm, respectively. The distance and the DC bias between the nozzle and the substrates were set to 21 cm and 8 kV, respectively. The environmental conditions were a temperature of 14 °C and 3.6% relative humidity. The AgNFs were formed by coalescing the Ag nanoparticles by heating at 150 °C for 30 minutes. Subsequently, the AgNW (Flexio Co., Ltd.) had an average diameter of 30 ± 5 nm and an average length of 25 ± 5 μm, and it was electrosprayed for 1 minute on the substrate on which the AgNF was electrospun at the following conditions. The distance and the DC bias between the nozzle and the substrates were set to 13 cm and 9.5 kV, respectively. The diameter of the nozzle was 0.33 mm. The AgNF-AgNW electrodes were photolithographically patterned through a wet-etching process.

Fabrication process of the smart contact lenses

Parylene was deposited as a passivation layer on the Ni/Cu (10/800 nm) sacrificial layer. A Cr/Au (5/100 nm) electrode was deposited through e-beam evaporation and patterned as antenna pads and source and drain of the FET-type sensor. The AgNF-AgNW hybrid electrode was deposited by electrospinning and patterned to the antenna coil. Rigid material (Optical polymer) was patterned to a rigid region on the sensor. Soft material (Elastofilcone A) was coated on the entire sample area. The sacrificial layer was removed through wet etching. The sample was lifted-off from the substrate and attached in the reverse position to the handling layer. Parylene was patterned through RIE etching (100 W, 180 seconds) to open holes on the pads of the antenna and the sensor. Graphene was transferred onto the sensor to make the graphene channel. Graphene was patterned to make the channel of the sensor through RIE etching (50 W, 30 s). The NFC chip, a capacitor, and a resistor were bonded to the sample with lens material. All of the components were integrated through 3D printing. The sensor was protected with a PDMS stamp before molding the lens. Lens material and the fabricated device were casted together into the lens mold at a pressure of 313 kPa and cured at 70 °C for 4 hours. The smart contact lens was completed after

removing the PDMS stamp and functionalizing the cortisol sensor by dropping EDC, NHS and C-Mab solutions.

Thermal characterization
For the thermal characterization during the *in-vivo* test, the temperature was measured by an LWIR camera (T650sc, FLIR Systems, Wilsonville, OR, USA). The temperature distributions of the images and the video were analyzed using FLIR ResearchIR software (Research IR Max, FLIR Systems).

Electrical characterization
The four-point probe method was used for the measurement of the sheet resistance using a probe station with a Keithley 4200-SCS semiconductor parametric analyzer. The electrical characteristics of graphene and the real-time sensing of the cortisol sensor were conducted using a probe station (Keithley 4200-SCS).

Optical characterization
The optical transparency was measured by an UV/Vis spectrophotometer (Cary 5000 UV-vis-NIR, Agilent). SEM images were obtained by field emission scanning electron microscope (JEOL, IT-500HR).

Fourier-transform infrared spectroscopy (FT-IR)
The FT-IR spectra of the samples were obtained using an FT-IR spectrometer (Vertex 70, Bruker) at 25 °C, with an attenuated total reflectance (ATR) stage. All of the spectra in the 256 scans were recorded between 4000 and 1000 cm^{-1} with a resolution of 4 cm^{-1}.

Microfluidic channel for real-time sensing of cortisol A negative photoresist (PR) was patterned to the structure of the inside of the microfluidic channel. Subsequently, the PDMS (Sylgard 184 silicone elastomer: curing agent = 10:1 wt%) was cured on the patterned negative PR. Separating the PDMS from the negative PR, the microfluidic channel was completed by drilling holes for the injection of the solution. The PDMS microfluidic channel was located on the sensor, and the diluted cortisol solution (Sigma-Aldrich., #C-106, various concentrations) and the buffer solution (Samchun Pure Chemical Co., pH7.00 ± 0.02) were injected to the microfluidic channel with a syringe pump (New Era Pump Systems, Inc., NE-300). The amount of biofluid can be calculated using the flow rate (1 ml/h) and the response time of the sensor (3 seconds). The response time, i.e., the time required for the level of the current to reach 90% of the saturated level at a cortisol concentration of 1 ng/ml, was calculated from Fig. 2A. Therefore, the minimum volume of biofluid required to detect the cortisol was only 0.83 µl, i.e., 1 ml/hour × 3 sec × 1 hr/3600 sec × 1000 µl/ml, which was less than the volume of a tear, i.e., 1 µl (*1*).

Selectivity test
For the selectivity test, the sensor is tested by the solutions of 1 – 40 ng/ml cortisol with 50 µM ascorbic acid (Product #PHR1008, Sigma-Aldrich), 10 mM lactate (Product #PHR1113, Sigma-Aldrich), and 10 mM urea (Product #PHR1406, Sigma-Aldrich).

Accelerated aging tests for the antenna
In the accelerated aging test, the accelerated aging time can be determined by Equation (1),

$$Accelerated\ aging\ time = \frac{Desired\ real\ time}{Q_{10}^{[(T_{AA}-T_{AMB})/10]}} \quad (1)$$

where Q_{10}, T_{AA}, and T_{AMB} are the aging factor (~2), the accelerated aging temperature (70 °C), and the ambient temperature, respectively (*2*). For the storage period of 1 year, the T_{AMB} was assumed to be room temperature (25 °C), and therefore the accelerated aging time was calculated to be 16 days. According to these calculations, our contact lens device was stored in air for up to 16 days.

Specific absorption rate (SAR) simulation

Finite element analysis was conducted to simulate the maximum SAR for a person. The simulations were performed using commercial software, i.e., Ansoft HFSS. In the simulation, the antenna was located under the model of the human head, and the transmitting power from the transmitter or the smartphone was set as 10 W for the extreme environment test.

Embedding of the integrated wireless circuit into a soft contact lens

The fully-integrated device, including the cortisol sensor, antenna coil, NFC chip, reference resistor, and capacitor, was embedded into the lens material. The fabricated device and lens material were put together on the lens mold and cured at 100 ºC for 1 hour at a pressure of 313 kPa. Subsequently, the soft lens that was embedded with the device was separated from the mold.

Slit lamp examination in a human study

The protocol for this study was approved by the Institutional Review Board of UNIST (UNISTIRB-18-17-A), and the participant gave informed consent. The smart contact lens was rinsed using a commercially-available cleaning solution for contact lens (Frenz-pro B5 solution, JK Pharmaceutical Inc., Korea), followed by additional rinsing using a PBS solution for one minute before wearing. This examination was performed after the lens had been worn for 12 hours. After the human trial, the ocular surface of the volunteer was evaluated using the slit lamp examination (SL-15, Kowa Optimed Inc., Japan).

PDMS stamp to protect the sensor

A negative photoresist (PR) was patterned to the structure of the inside of the stamp. Subsequently, the PDMS (Sylgard 184 silicone elastomer: curing agent = 10:1 wt%) was cured on the patterned negative PR. The PDMS stamp was formed by separating the PDMS from the negative PR.

Supplementary Materials

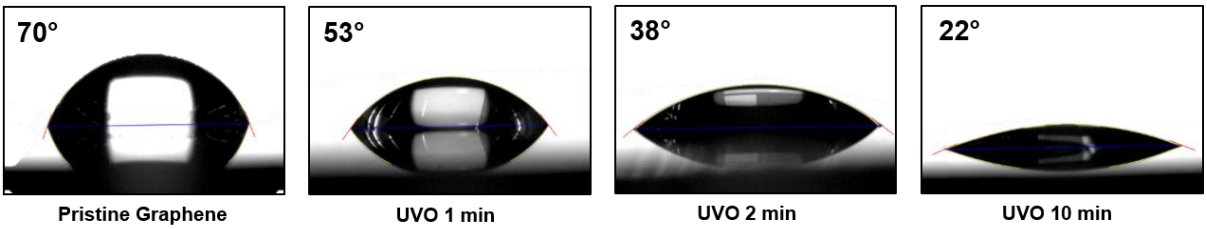

Fig. S1. Characteristic change of the graphene surface. Contact angle between a 1-μl droplet of deionized water and the pristine and UVO exposed graphene. The contact angle was reduced by increasing the exposure time of the UVO.

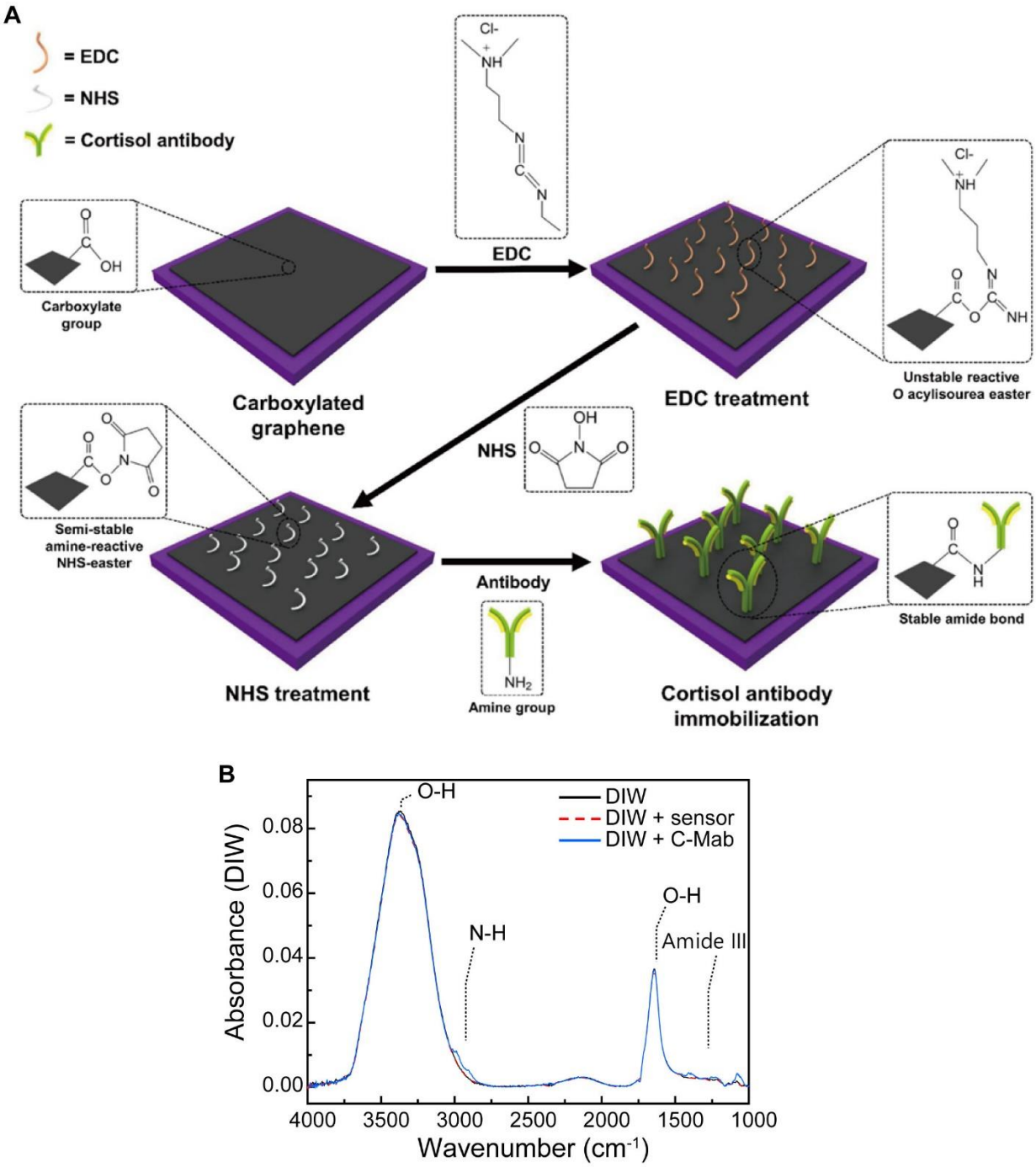

Fig. S2. C-Mab immobilization. (A) The process of immobilizing C-Mab through the EDC/NHS coupling reaction. Pristine graphene is carboxylated by UVO exposure. Then, Carboxlated graphene is covalently bonded with EDC (1-ethyl-3-(3-dimethylaminopropyl)carbodiimide hydrochloride) and becomes unstable. After N-hydroxysulfosuccinimide (NHS) treatment, it is in a semi-stable state. C-Mab is immobilized to the semi-stable NHS and becomes stable. **(B)** FT-IR spectra of the deionized water after the immersion of the cortisol sensor (red), pristine deionized water without immersion (black), and the solution of 1 μg/ml cortisol monoclonal antibody (blue).

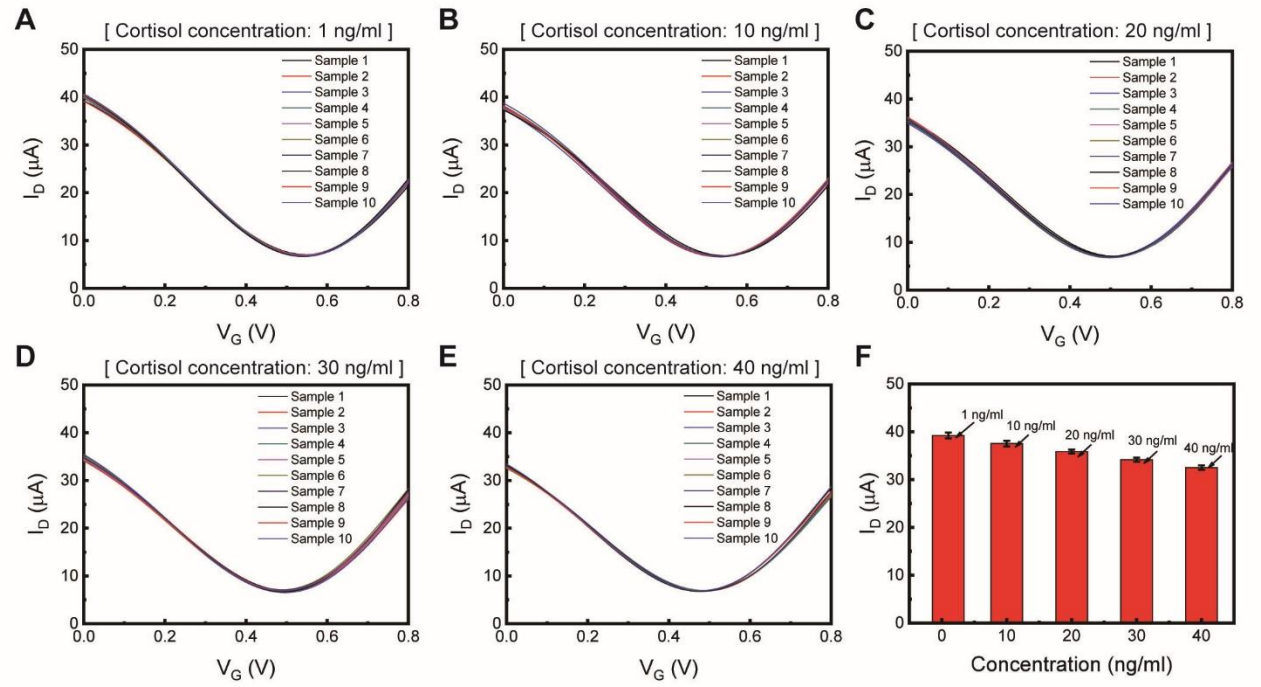

Fig. S3. Reproducibility tests. I_D-V_G (transfer) curves of all graphene transistor samples **(A)** at a cortisol concentration of 1 ng/ml, **(B)** at a cortisol concentration of 10 ng/ml, **(C)** at a cortisol concentration of 20 ng/ml, **(D)** at a cortisol concentration of 30 ng/ml, **(E)** at a cortisol concentration of 40 ng/ml. **(F)** Absolute drain current values according to the cortisol concentration. Each data point indicates the average for 10 samples, and the error bars represent the standard deviations.

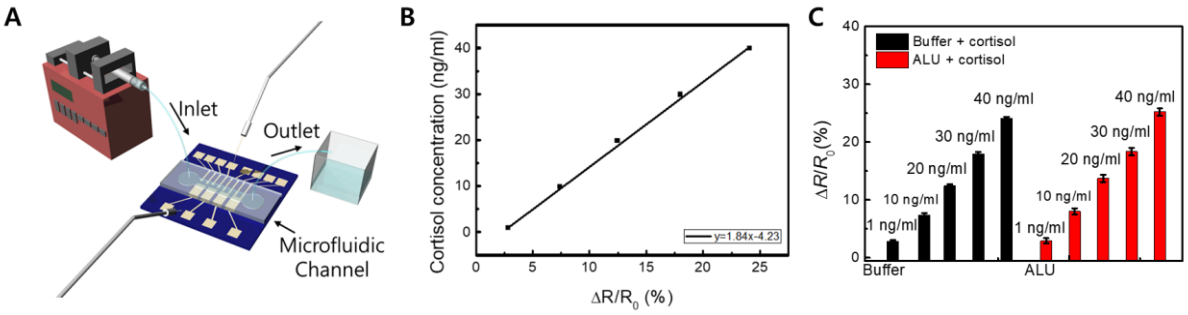

Fig. S4. Cortisol sensor characteristic tests. (A) Schematic illustration of the real-time cortisol sensing using a microfluidic channel. **(B)** Calibration curve of the cortisol sensor characteristic calculated with resistance change. **(C)** Relative changes in the resistance of the cortisol sensor according to the cortisol concentration in the buffer solution (black) and ALU solution (A: 50 μM ascorbic acid, L: 10 mM lactate, U: 10 mM urea) (red). Each data point indicates the average for 10 samples, and the error bars represent the standard deviations.

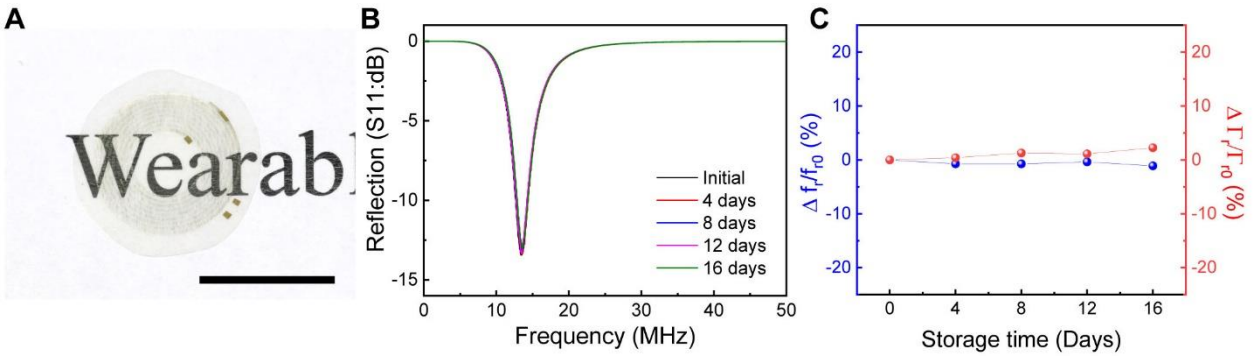

Fig. S5. Antenna characteristic tests. (A) Photograph of the AgNF-AgNW antenna of 71% transparency. Scale bar, 1 cm. **(B)** Resonance properties of the antenna for 16 days under the 70 °C air condition. **(C)** Relative change in the resonance frequency (blue) and relative change in the reflection coefficient (red) of the antenna from Fig. S5B. Photo credit: (A) Minjae Ku, Yonsei University.

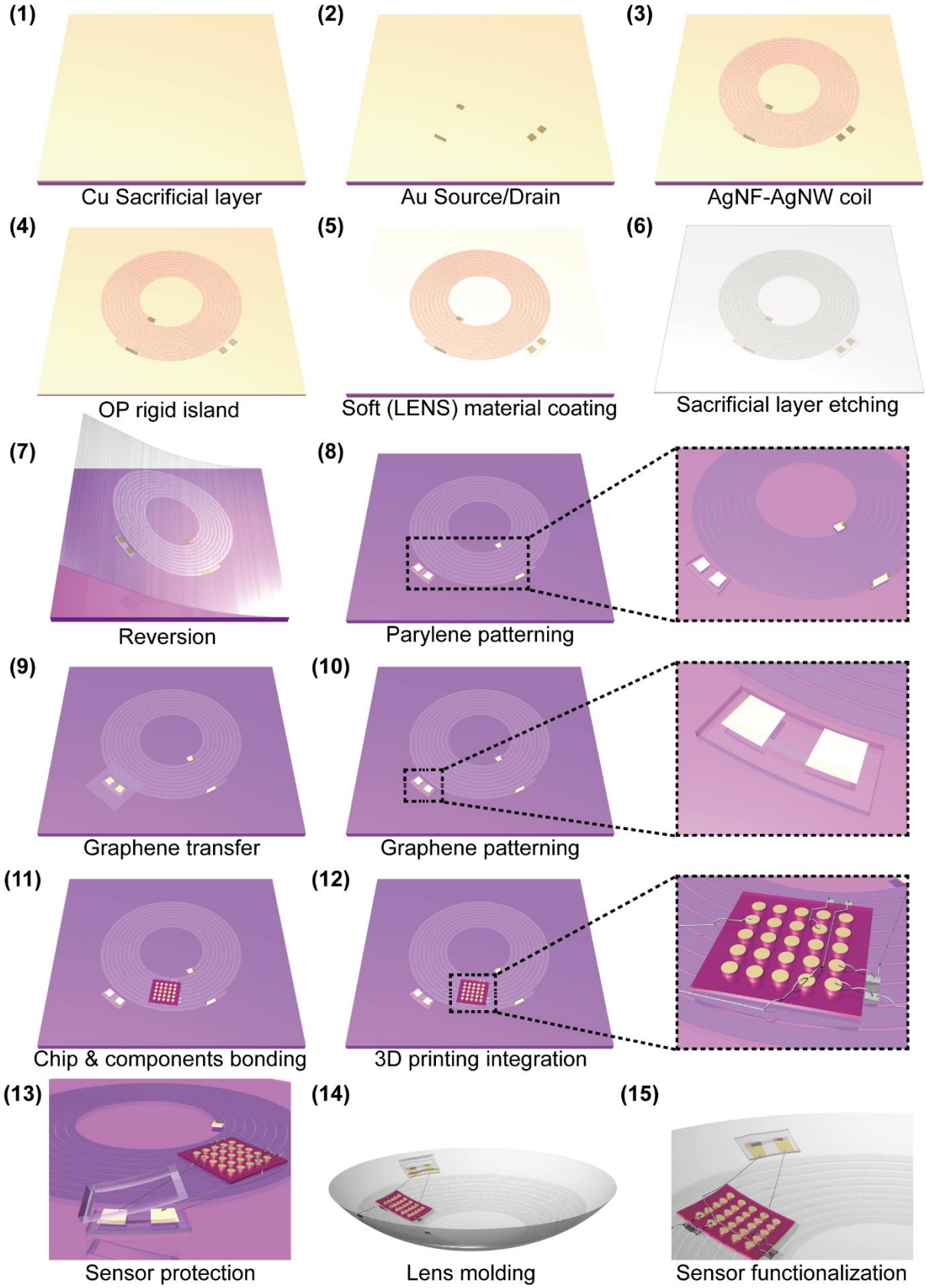

Fig. S6. Fabrication process and materials of smart contact lenses.

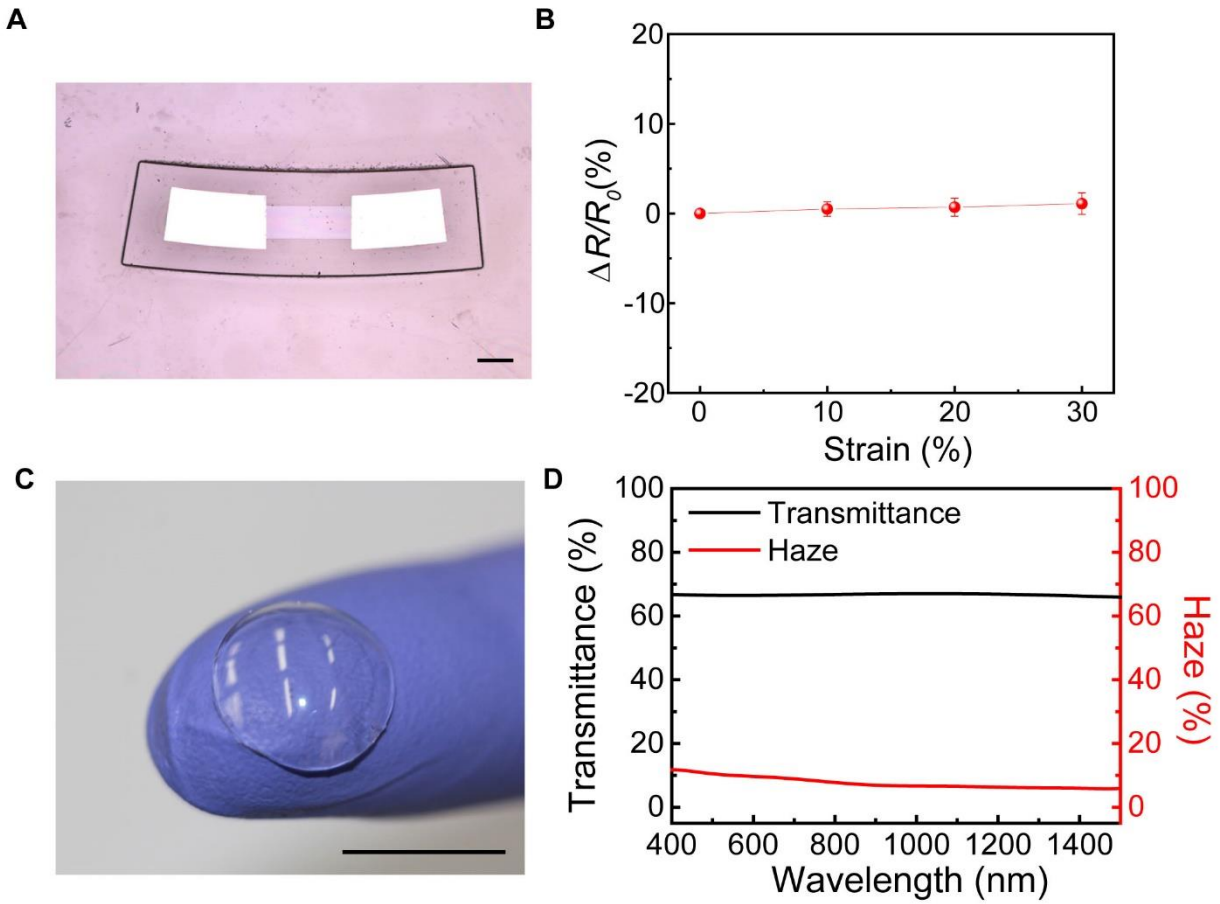

Fig. S7. Rigid-soft hybrid substrate characteristic tests. (A) Photograph of the cortisol sensor on the rigid island. The scale bar is 200 μm. **(B)** Relative change in the resistance of the cortisol sensor as a function of tensile strain. **(C)** Photograph of the lens embedded with the rigid-soft hybrid substrate. The optical transparency and haze were measured as 93% and 1.2%, respectively (at 550 nm). The scale bar is 1 cm. Photo credit: Minjae Ku, Yonsei University. **(D)** Optical properties of integrated contact lens. Transmittance (black) and haze (red) spectra of the smart contact lens.

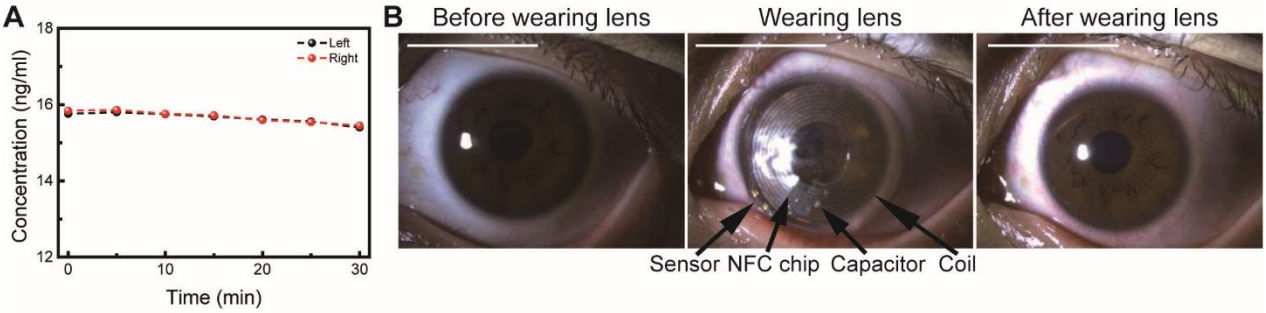

Fig. S8. ***In-vivo*** **tests on a human. (A)** Variation of the cortisol concentrations measured in both eyes of a human subject using the smart contact lens. **(B)** Slit lamp examination of a human eye: The slit lamp images were taken before, during, and after wearing the smart contact lens. Scale bars, 1 cm. Photo credits: Minjae Ku, Yonsei University.

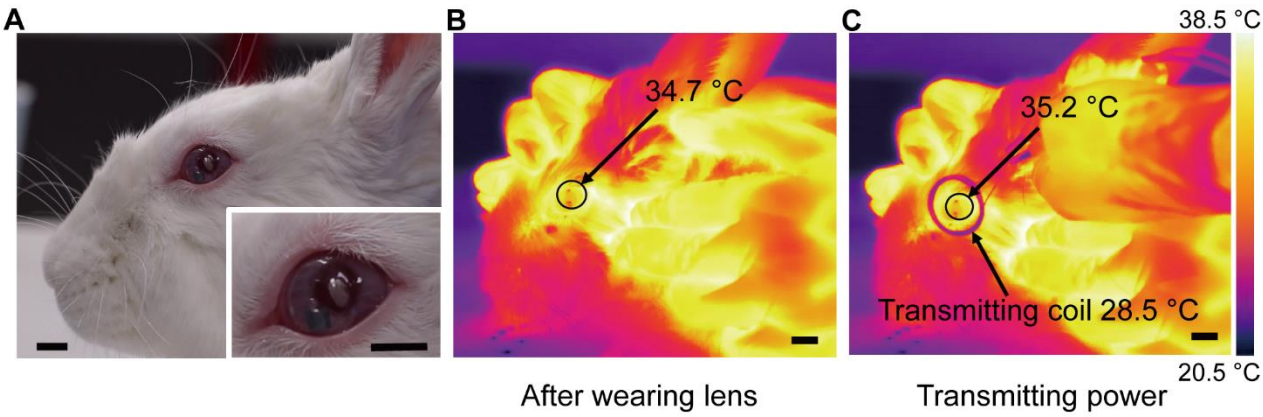

Fig. S9. ***In-vivo*** **tests on a rabbit. (A)** Smart contact lens on the eye of a live rabbit. (Inset: close-up image of the rabbit's eye.) Scale bars, 1 cm. **(B, C)** Thermal analyses of the radiation of the antenna against the transmitted power. Scale bars, 2 cm. Photo credits: (A to C) Minjae Ku, Yonsei University.

		Sample 1 (UVO 1 min)	Sample 2 (UVO 2 min)	Sample 4 (UVO 10 min)
Before UVO	**Resistance (Ω)**	109	162	1200
	Contact angle (°)	70	71	70
After UVO	**Resistance (Ω)**	110	260	2000
	Contact angle(°)	53	38	22

Table S1. Table of contact angle and resistance according to the UVO exposure time.

Movie S1 (.avi format). Real-time measurement of cortisol level for a 24-year-old female using the smart contact lens sensor.

Movie S2 (.avi format). Real-time monitoring of a rabbit using the smart contact lens sensor.

Movie S3 (.avi format). *In-vivo* test conducted using a live rabbit for monitoring the generation of heat during the wireless operation of the smart lens.

REFERENCES AND NOTES

1. F. Holsboer, M. Ising, Stress hormone regulation: Biological role and translation into therapy. *Annu. Rev. Psychol.* **61**, 81–109 (2010).

2. E. R. de Kloet, M. Joëls, F. Holsboer, Stress and the brain: From adaptation to disease. *Nat. Rev. Neurosci.* **6**, 463–475 (2005).

3. S. H. Sunwoo, J. S. Lee, S. Bae, Y. J. Shin, C. S. Kim, S. Y. Joo, H. S. Choi, M. Suh, S. W. Kim, Y. J. Choi, T.-i. Kim, Chronic and acute stress monitoring by electrophysiological signals from adrenal gland. *Proc. Natl. Acad. Sci. U.S.A.* **116**, 1146–1151 (2019).

4. J. Newell-Price, X. Bertagna, A. B. Grossman, L. K. Nieman, Cushing's syndrome. *Lancet* **367**, 1605–1617 (2006).

5. L. Stojanovich, Stress and autoimmunity. *Autoimmun. Rev.* **9**, A271–A276 (2010).

6. B. S. McEwen, Protective and damaging effects of stress mediators. *N. Engl. J. Med.* **338**, 171–179 (1998).

7. F. A. J. L. Scheer, M. F. Hilton, C. S. Mantzoros, S. A. Shea, Adverse metabolic and cardiovascular consequences of circadian misalignment. *Proc. Natl. Acad. Sci. U.S.A.* **106**, 4453–4458 (2009).

8. O. M. Edwards, R. J. Courtenay-Evans, J. M. Galley, J. Hunter, A. D. Tait, Changes in cortisol metabolism following rifampicin therapy. *Lancet* **2**, 548–551 (1974).

9. X. Saichan, C. Wei, F. Qinglong, W. Jun, X. Lei, Plasma cortisol as a noninvasive biomarker to assess severity and prognosis of patients with craniocerebral injury. *Eur. Rev. Med. Pharmacol. Sci*. **20**, 3835–3838 (2016).

10. R. Thun, E. Eggenberger, K. Zerobin, T. Lüscher, W. Vetter, Twenty-four-hour secretory pattern of cortisol in the bull: Evidence of episodic secretion and circadian rhythm. *Endocrinology* **109**, 2208–2212 (1981).

11. R. M. Sapolsky, Individual differences in cortisol secretory patterns in the wild baboon: Role of negative feedback sensitivity. *Endocrinology* **113**, 2263–2267 (1983).

12. A. Kaushik, A. Vasudev, S. K. Arya, S. K. Pasha, S. Bhansali, Recent advances in cortisol sensing technologies for point-of-care application. *Biosens. Bioelectron.* **53**, 499–512 (2014).

13. P. K. Vabbina, A. Kaushik, N. Pokhrel, S. Bhansali, N. Pala, Electrochemical cortisol immunosensors based on sonochemically synthesized zinc oxide 1D nanorods and 2D nanoflakes. *Biosens. Bioelectron.* **63**, 124–130 (2015).

14. A. Singh, A. Kaushik, R. Kumar, M. Nair, S. Bhansali, Electrochemical sensing of cortisol: A recent update. *Appl. Biochem. Biotech.* **174**, 1115–1126 (2014).

15. O. Parlak, S. T. Keene, A. Marais, V. F. Curto, A. Salleo, Molecularly selective nanoporous membrane-based wearable organic electrochemical device for noninvasive cortisol sensing. *Sci. Adv.* **4**, eaar2904 (2018).

16. D. Kinnamon, R. Ghanta, K.-C. Lin, S. Muthukumar, S. Prasad, Portable biosensor for monitoring cortisol in low-volume perspired human sweat. *Sci. Rep*. **7**, 13312 (2017).

17. Y.-H. Kim, K. Lee, H. Jung, H. K. Kang, J. Jo, I.-K. Park, H. H. Lee, Direct immune-detection of cortisol by chemiresistor graphene oxide sensor. *Biosens. Bioelectron.* **98**, 473–477 (2017).

18. T. Stalder, S. Steudte, N. Alexander, R. Miller, W. Gao, L. Dettenborn, C. Kirschbaum, Cortisol in hair, body mass index and stress-related measures. *Biol. Psychol.* **90**, 218–223 (2012).

19. S. K. Arya, A. Dey, S. Bhansali, Polyaniline protected gold nanoparticles based mediator and label free electrochemical cortisol biosensor. *Biosens. Bioelectron.* **28**, 166–173 (2011).

20. N. M. Farandos, A. K. Yetisen, M. J. Monteiro, C. R. Lowe, S. H. Yun, Contact lens sensors in ocular diagnostics. *Adv. Healthc. Mater.* **4**, 792–810 (2015).

21. B. A. Cardinell, M. L. Spano, J. T. La Belle, Toward a label-free electrochemical impedance immunosensor design for quantifying cortisol in tears. *Crit. Rev. Biomed. Eng*. **47**, 207–215 (2019).

22. J. Park, D. B. Ahn, J. Kim, E. Cha, B.-S. Bae, S.-Y. Lee, J.-U. Park, Printing of wirelessly rechargeable solid-state supercapacitors for soft, smart contact lenses with continuous operations. *Sci. Adv.* **5**, eaay0764 (2019).

23. J. Kim, M. Kim, M.-S. Lee, K. Kim, S. Ji, Y.-T. Kim, J. Park, K. Na, K.-H. Bae, H. K. Kim, F. Bien, C. Young Lee, J.-U. Park, Wearable smart sensor systems integrated on soft contact lenses for wireless ocular diagnostics. *Nat. Commun.* **8**, 14997 (2017).

24. J. Kim, E. Cha, J. Park, Recent advances in smart contact lenses. *Adv. Mater. Technol.* **5**, 1900728 (2020).

25. J. Kim, J. Kim, M. Ku, E. Cha, S. Ju, W. Y. Park, K. H. Kim, D. W. Kim, P.-O. Berggren, J.-U. Park, Intraocular pressure monitoring following islet transplantation to the anterior chamber of the eye. *Nano Lett.* **20**, 1517–1525 (2020).

26. L. K. Banbury, "Stress biomarkers in the tear film," thesis, Southern Cross University, Lismore, NSW (2009).

27. C. Tlili, N. V. Myung, V. Shetty, A. Mulchandani, Label-free, chemiresistor immunosensor for stress biomarker cortisol in saliva. *Biosens. Bioelectron.* **26**, 4382–4386 (2011).

28. J. Kim, M.-S. Lee, S. Jeon, M. Kim, S. Kim, K. Kim, F. Bien, S. Y. Hong, J.-U. Park, Highly transparent and stretchable field-effect transistor sensors using graphene-nanowire hybrid nanostructures. *Adv. Mater.* **27**, 3292–3297 (2015).

29. M. T. Hwang, M. Heiranian, Y. Kim, S. You, J. Leem, A. Taqieddin, V. Faramarzi, Y. Jing, I. Park, A. M. van der Zande, S. Nam, N. R. Aluru, R. Bashir, Ultrasensitive detection of nucleic acids using deformed graphene channel field effect biosensors. *Nat. Commun.* **11**, 1543 (2020).

30. B. Cai, S. Wang, L. Huang, Y. Ning, Z. Zhang, G.-J. Zhang, Ultrasensitive label-free detection of PNA–DNA hybridization by reduced graphene oxide field-effect transistor biosensor. *ACS Nano* **8**, 2632–2638 (2014).

31. T.-Y. Chen, P. T. K. Loan, C.-L. Hsu, Y.-H. Lee, J. T.-W. Wang, K.-H. Wei, C.-T. Lin, L.-J. Li, Label-free detection of DNA hybridization using transistors based on CVD grown graphene. *Biosens. Bioelectron.* **41**, 103–109 (2013).

32. E. Fernandes, P. D. Cabral, R. Campos, G. Machado Jr, M. F. Cerqueira, C. Sousa, P. P. Freitas, J. Borme, D. Y. Petrovykh, P. Alpuim, Functionalization of single-layer graphene for immunoassays. *Appl. Surf. Sci.* **480**, 709–716 (2019).

33. H. Tao, M. A. Brenckle, M. Yang, J. Zhang, M. Liu, S. M. Siebert, R. D. Averitt, M. S. Mannoor, M. C. McAlpine, J. A. Rogers, D. L. Kaplan, F. G. Omenetto, Silk-based conformal, adhesive, edible food sensors. *Adv. Mater.* **24**, 1067–1072 (2012).

34. J. Kim, A. Banks, Z. Xie, S. Y. Heo, P. Gutruf, J. W. Lee, S. Xu, K.-I. Jang, F. Liu, G. Brown, J. Choi, J. H. Kim, X. Feng, Y. Huang, U. Paik, J. A. Rogers, Miniaturized flexible electronic systems with wireless power and near-field communication capabilities. *Adv. Funct. Mater.* **25**, 4761–4767 (2015).

35. G. E. Dunbar, B. Shen, A. Aref, The Sensimed Triggerfish contact lens sensor: Efficacy, safety, and patient perspectives. *Clin. Ophthalmol.* **11**, 875–882 (2017).

36. S. Cheng, Z. Wu, A microfluidic, reversibly stretchable, large-area wireless strain sensor. *Adv. Funct. Mater.* **21**, 2282–2290 (2011).

37. J. Mujal, E. Ramon, E. Díaz, J. Carrabina, Á. Calleja, R. Martínez, L. Terés, Inkjet printed antennas for NFC systems, in *17th IEEE International Conference on Electronics, Circuits and System* (IEEE, 2010), pp. 1220–1223.

38. J. Jang, B. G. Hyun, S. Ji, E. Cho, B. W. An, W. H. Cheong, J.-U. Park, Rapid production of large-area, transparent and stretchable electrodes using metal nanofibers as wirelessly operated wearable heaters. *NPG Asia Mater*. **9**, e432 (2017).

39. M. H. Tooley, M. H. Tooley, *Electronic Circuits: Fundamentals and Applications* (Elsevier, ed. 3, 2006), pp. 77–78.

40. Y.-G. Park, H. Min, H. Kim, A. Zhexembekova, C. Y. Lee, J.-U. Park, Three-dimensional, high-resolution printing of carbon nanotube/liquid metal composites with mechanical and electrical reinforcement, *Nano Lett.* **19**, 4866–4872 (2019).

41. Y.-G. Park, H. S. An, J.-Y. Kim, J.-U. Park, High-resolution, reconfigurable printing of liquid metals with three-dimensional structures. *Sci. Adv.* **5**, eaaw2844 (2019).

42. J. Park, J. Kim, S.-Y. Kim, W. H. Cheong, J. Jang, Y.-G. Park, K. Na, Y.-T. Kim, J. H. Heo, C. Y. Lee, J. H. Lee, F. Bien, J.-U. Park, Soft, smart contact lenses with integrations of wireless circuits, glucose sensors, and displays. *Sci. Adv.* **4**, eaap9841 (2018).

43. IEEE standard for safety levels with respect to human exposure to radio frequency electromagnetic fields, 3 kHz to 300 GHz, in *IEEE Std C95.1-2005 (Revision of IEEE Std C95.1-1991)* (IEEE, 2006), pp. 1–238.

44. A. Comin, V. Zufferli, T. Peric, F. Canavese, D. Barbetta, A. Prandi, Hair cortisol levels determined at different body sites in the New Zealand White rabbit. *World Rabbit Sci.* **20**, 149–154 (2012).

45. E. J. Holland, M. J. Mannis, W. B. Lee, *Ocular Surface Disease: Cornea, 158 Conjunctiva and Tear Film* (Elsevier/Saunders, London, 2013), 159 pp.

46. American Society for Testing Materials, Standard Guide for Accelerated Aging of 160 Sterile Barrier Systems for Medical Devices. ASTM F1980-07 (2011).